International Journal of Mass Spectrometry 295 (2010) 65–71

Contents lists available at ScienceDirect

International Journal of Mass Spectrometry

journal homepage: www.elsevier.com/locate/ijms

Dissociation of the thiophenol molecular ion: A theoretical study

Sun Young Kim, Joong Chul Choe*

Department of Chemistry, Dongguk University-Seoul, Seoul 100-715, Republic of Korea

ARTICLE INFO

Article history:
Received 31 May 2010
Received in revised form 5 July 2010
Accepted 6 July 2010
Available online 12 July 2010

Keywords:
Potential energy surface
G3//B3LYP
RRKM calculation
Kinetics
Reaction pathway

ABSTRACT

The potential energy surface (PES) for the losses of H•, SH•, C_2H_2, and CS from the thiophenol molecular ion was determined from the G3//B3LYP calculations. Several rearrangement pathways including ring expansion, contraction, and opening were found for the losses of C_2H_2 and CS. Rice–Ramsperger–Kassel–Marcus model calculations were carried out based on the PES in order to examine the competition between the losses of C_2H_2 and CS. From the kinetic analysis it was predicted that the loss of C_2H_2 was more favored at low energies and the loss of CS was more favored at high energies, which is in agreement with previous experimental results.

1. Introduction

Dissociations of ionized monosubstituted benzenes have been extensively studied using various experimental and theoretical methods. Recently, dissociation mechanisms of the molecular ions of $C_6H_5XH_n$ (X = C, Si, N, P, and O) were proposed on the basis of quantum chemical calculations [1–7]. Interestingly, ring expansion, contraction, and opening all play important roles in the dissociations of such molecular ions. It is well known that the formation of the tropylium ion from the toluene molecular ion, $C_6H_5CH_3^{+\bullet}$, occurs through isomerization by ring expansion followed by elimination of H• [1,2]. In contrast, it was proposed that the seven-membered ring isomer of the phenylsilane molecular ion, $C_6H_5SiH_3^{+\bullet}$, would hardly contribute to the loss of H• [3]. Similarly, ring expansion is not important in the dissociations of the aniline and phenylphosphine molecular ions ($C_6H_5NH_2^{+\bullet}$ and $C_6H_5PH_2^{+\bullet}$) [4–6]. Instead, ring contraction to the five-membered ring isomers plays an important role in the formation of the cyclopentadiene radical cation ($CP^{+\bullet}$) by loss of HNC [5] or HCP [6]. For the phenylphosphine ion, the seven-membered ring intermediate isomerizes to the five-membered isomer before the loss of HCP. In its secondary dissociation, the loss of HCP or C_2H_2 from $C_6H_5PH^+$ also occurs through consecutive isomerizations to the seven- and five-membered ring isomers. Le et al. reported a theoretical potential energy surface (PES) for the loss of CO from the phenol molecular ion, $C_6H_5OH^{+\bullet}$ [7]. Ring opening and contraction are involved in the reported lowest energy pathway for the loss of CO to form $CP^{+\bullet}$.

Rearrangement of an α-H to the benzene ring triggers ring expansion or contraction in $C_6H_5XH_n^{+\bullet}$ ions. The isomers formed by 1,2- and 1,3-H shifts become the precursors for ring expansion and contraction, respectively (Scheme 1). The 1,3-H shift can occur through consecutive 1,2- and *ipso*-to-*ortho*-H shifts.

The thiophenol molecular ion ($C_6H_5SH^{+\bullet}$, **1**) undergoes primary dissociations to four major fragment ions by losses of H•, SH•, C_2H_2, and CS according to studies using electron ionization (EI) mass spectrometry [8,9]; this is in contrast to the phenol molecular ion that dissociates mainly to $CP^{+\bullet}$ + CO [7,8]. Deuterium labeling [9,10], ion cyclotron resonance (ICR) [11,12], and photoionization (PI) [11] mass spectrometry have been used to study the kinetics and mechanisms of the dissociation of **1**. Faulk et al. [11] proposed a mechanism for the loss of CS, where a 1,3-H shift and ring contraction are involved. In this work, a theoretical PES was examined for the primary dissociations of **1**. Various dissociation pathways were found. The dissociation kinetics is discussed based on the PES.

2. Computational methods

The molecular orbital calculations were performed with the Gaussian 09 suite of programs [13]. The geometry of the minima was optimized at the unrestricted B3LYP level of the DFT using the 6-31G(d) basis set. The transition state (TS) geometries that connected the stationary points were examined and checked by calculating the intrinsic reaction coordinates at the same level. For better accuracy of the energies, Gaussian-3 (G3) theory calculations

Abbreviations: PES, potential energy surface; $CP^{+\bullet}$, cyclopentadiene radical cation; TS, transition state; $TP^{+\bullet}$, thiophene radical cation.

* Corresponding author. Tel.: +82 2 2260 8914; fax: +82 2 2268 8204.
E-mail address: jcchoe@dongguk.edu (J.C. Choe).

1387-3806/$ – see front matter © 2010 Elsevier B.V. All rights reserved.
doi:10.1016/j.ijms.2010.07.005

Table 1
The total energy at 0 K, E_{tot}, the enthalpy at 298 K, H°_{298}, the relative energy at 0 K, ΔE_{tot}, the enthalpy of reaction at 298 K, $\Delta_r H^{\circ}_{298}$, and the experimental enthalpy of reaction at 298 K, $\Delta_r H^{\circ}_{298,exptl}$.

Species	G3//B3LYP calculation				$\Delta_r H^{\circ}_{298,exptl}$, kJ mol^{-1} [a]
	E_{tot}, hatrees	H°_{298}, hatrees	ΔE_{tot}, kJ mol^{-1}	$\Delta_r H^{\circ}_{298}$, kJ mol^{-1}	
1	−629.804719	−629.797510	0	0	0
$TP^{+\bullet} + C_2H_2$	−629.700499	−629.691179	274	279	286
$CP^{+\bullet} + CS$	−629.684538	−629.675856	316	319	319
$C_6H_5S^+ + H^{\bullet}$	−629.677786	−629.668522	333	339	
$C_6H_5^+ + SH^{\bullet}$	−629.671359	−629.662090	350	356	353

[a] From the experimental enthalpies of formation at 298 K in Ref. [19] except for that of $CP^{+\bullet}$ from Ref. [8].

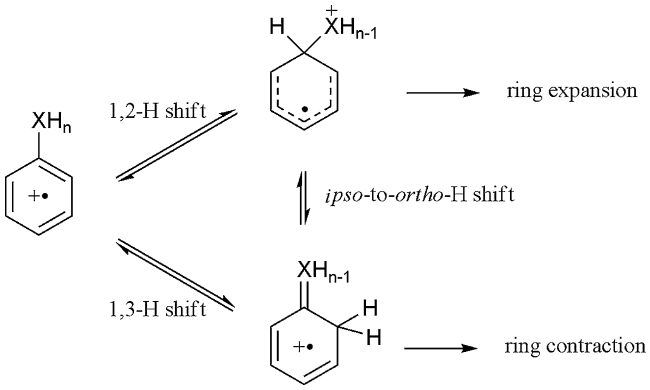

Scheme 1.

using the B3LYP density functional method (G3//B3LYP) [14] were performed. In G3//B3LYP calculations, the geometries are obtained at the B3LYP/6-31G(d) level, and the zero point vibrational energies are obtained at the same level and scaled by a factor of 0.96. All the other steps remain the same as the G3 method [15] with the exception of the values of the higher-level correction parameters.

The RRKM expression was used to calculate the rate-energy dependence for individual unimolecular reaction steps that were involved in the selected reaction pathways [16]:

$$k(E) = \frac{\sigma N^{\ddagger}(E - E_0)}{hp(E)} \quad (1)$$

In this equation, E is the internal energy of the reactant, E_0 is the critical energy of the reaction, $N^{\ddagger}$ is the sum of the TS states, ρ is the density of the reactant states, σ is the reaction path degeneracy, and h is Planck's constant. $N^{\ddagger}$ and ρ were evaluated through a direct count of the states using the Beyer–Swinehart algorithm [17].

The entropy of activation ($\Delta S^{\ddagger}$) at temperature T (K) for a reaction was calculated to characterize the 'looseness' of the TS using the following formula [18]:

$$\Delta S^{\ddagger} = k_B \ln \frac{Q^{\ddagger}}{Q} + \frac{V^{\ddagger} - V}{T} = k_B \ln \frac{\Pi q_i^{\ddagger}}{\Pi q_i} + \frac{V^{\ddagger} - V}{T} \quad (2)$$

where Q and q_i's are the total partition function and the molecular vibrational partition functions, respectively, V is the average vibra-

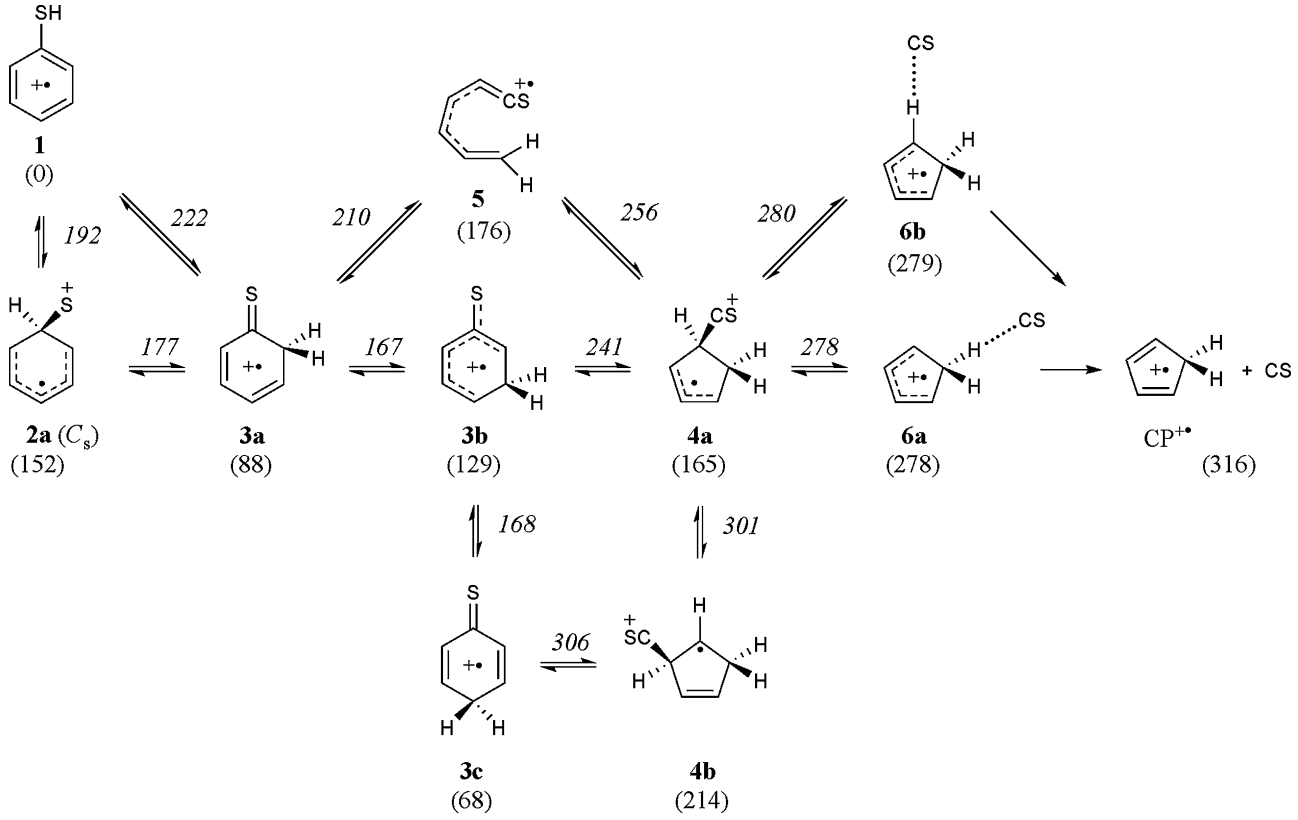

Scheme 2. The pathways for the loss of CS from **1** obtained from G3//B3LYP calculations. The calculated relative energies presented in kJ mol^{-1} are shown in the parentheses for the stable species and next to the arrows for the TS's.

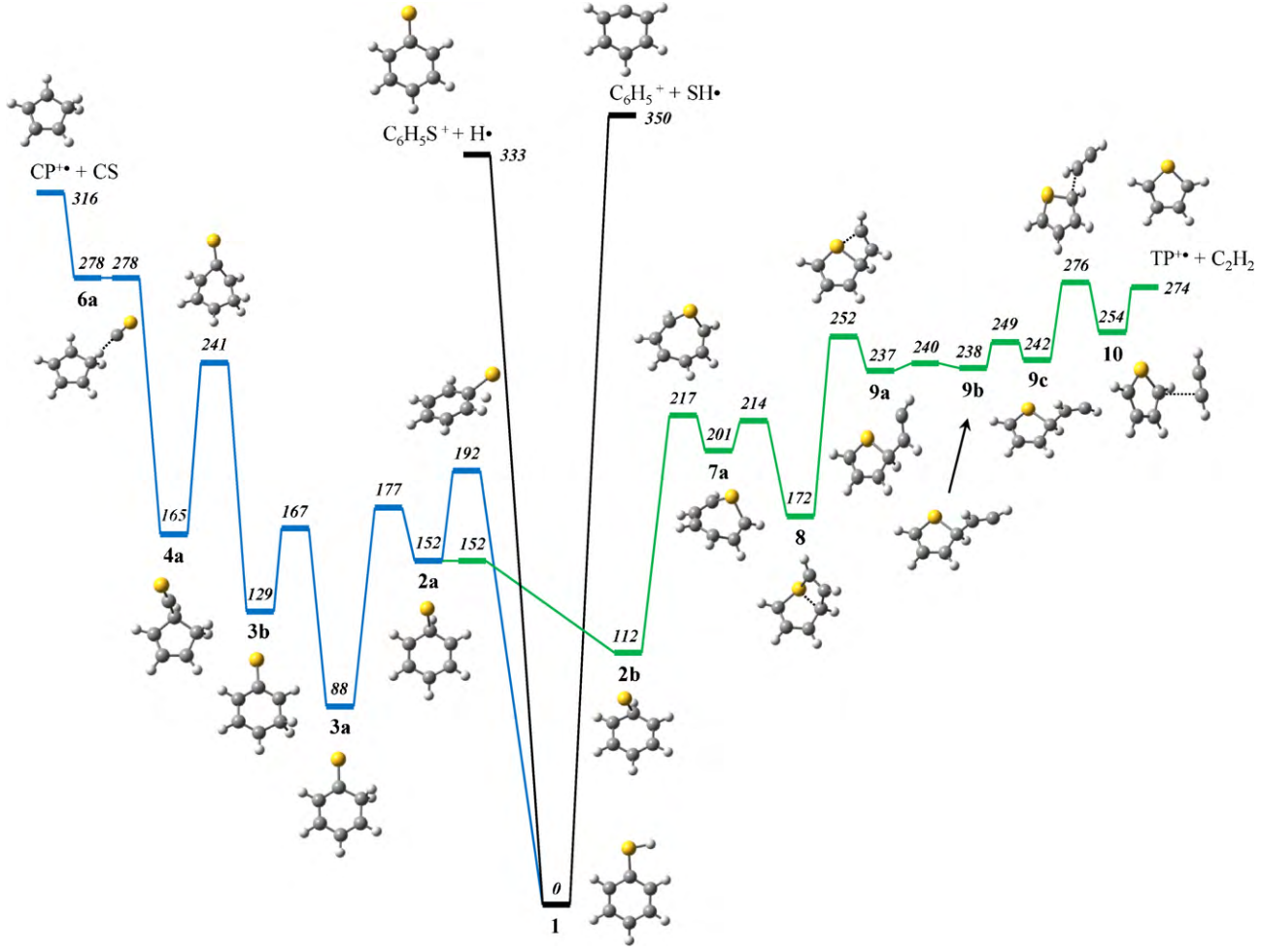

Fig. 1. Potential energy diagram for the lowest energy pathway of the dissociation of **1**, which was derived from G3//B3LYP calculations. The energies are presented in kJ mol^{-1}.

tional energy for the reactant, $Q^{\ddagger}$, $q_i^{\ddagger}$'s, and $V^{\ddagger}$ are the corresponding quantities for the TS, and k_B is the Boltzmann constant. The vibrational frequencies obtained from the B3LYP/6-31G(d) calculations were scaled down by a factor of 0.9614 and used for the calculations of k and $\Delta S^{\ddagger}$.

3. Results and discussion

1 optimized with the B3LYP/6-31G(d) calculation belongs to the point group C_S (see Fig. S1 and Table S1 in the supplementary material for the optimized structures of selected species), analogous to the phenol molecular ion [7]. The G3//B3LYP energies and enthalpies calculated for **1** and the main products are given in Table 1 together with their best literature enthalpy data [8,19]. The calculated enthalpies of reaction at 298 K agree with the experimental data within ±7 kJ mol^{-1}. The result shows that the loss of C_2H_2 is thermodynamically the most favorable among the four dissociation channels, the loss of CS is the second most, and the loss of SH• is the least favorable channel. The direct elimination of H• and SH• from **1** to form the phenylthiylium and phenylium ions, respectively, occur without reverse barriers. This was confirmed by scanning each PES at the B3LYP/6-31G(d) level.

For comparison purposes, the G3 calculations and single point energy calculations with the B3LYP, MP2, QCISD(T) methods were carried out for the selected species. The result is summarized in Table S2 of the supplementary material. For the present reactions, the relative G3 energies were similar to the relative G3//B3LYP energies, whereas the results of the single point energy calculations were largely deviated from the G3//B3LYP results that agreed with the experimental enthalpy data.

3.1. Reaction pathways

3.1.1. Loss of CS

Several pathways were found for the loss of carbon monosulfide, CS, to form CP+• (which appears to be the most stable $C_5H_6^{+\bullet}$ isomer) (Scheme 2). By a 1,2 shift of the α-H to the ipso position, **2a** is formed. By a further H shift to the ortho position, the *o*-isothiophenol radical cation (**3a**) is formed, which plays a role in the ring contraction. The 1,3-H shift can also occur directly. However, its barrier is higher than that for the consecutive H shifts. The H ring-walk proceeds to form the *m*- and *p*-isothiophenol radical cations, **3b** and **3c**, respectively. **3a** undergoes ring contraction through two different pathways. After isomerization to **3b**, the five-membered ring isomer (**4a**) is formed. Alternatively, **4a** can be formed from **3a** by consecutive ring cleavage and closure via **5**. **4a** isomerizes to two different ion–molecule complexes (**6a** and **6b**) before elimination of CS. CS is loosely attached to a H in the CH_2 group of **6a**, whereas it is attached to the H in the CH group of **6b**. These two pathways for the loss of CS from **4a** are almost energetically equivalent. **4a** can isomerize to **4b** by the CS or H ring-walk. The CS ring-walk is energetically favored. **3c** can form **4b** by ring contraction, but the corresponding TS lies much higher than that for **3b** → **4a**. These pathways for the loss of CS are similar to those for

the losses of CO [7] and HNC [5] from the phenol and aniline molecular ions, respectively. The lowest energy pathway for the loss of CS is shown in Fig. 1, which is different from those for the loss of CO or HNC where the ring opened intermediates analogous with **5** are included.

The barriers for the 1,2-H shift and subsequent H ring-walks (**1a** → **2a** → **3a** → **3b** → **3c**) are significantly lower than the energies required for dissociation, implying that the H scrambling occurs rapidly before dissociation at low energies. The occurrence of H scrambling before loss of H• was suggested in an early deuterium labeling study [9]. The mass spectrum of deuterated thiophenol, C_6H_5SD, shows the fragment peaks corresponding to $C_6H_5S^+$ and $C_6H_4DS^+$ with relative abundances of 10 and 13, respectively. It is also possible that the H scrambling is due to H ring-walks of the seven-membered ring isomers. The thia-cycloheptatriene radical cations (**7a**, **7b**) are formed after isomerization of **2a** to its slightly deformed isomer **2b** (Scheme 3). The planar isomer **7b** is more stable than the nonplanar **7a**. However, the barriers calculated for their H ring-walks (≥300 kJ mol^{-1} relative to **1**, not presented here) were much higher than those for the H ring-walks of the isothiophenol ions. This indicates that the seven-membered ring isomers would hardly contribute to the H scrambling.

In another mass spectrometric study with deuterium labeling [10], it was suggested that the loss of CS can occur after isomerization to the seven-membered ring isomers. This possibility seems unlikely because the H ring-walk needed inevitably before the elimination of CS from **7a** or **7b** requires much higher energy than that required for the loss of CS occurring through the isothiophenol ions.

3.1.2. Loss of C_2H_2

The loss of acethylene, C_2H_2, can occur from **7a** or **7b** by elimination of two adjacent carbons, α and β, β and γ, or two γ carbons. The elimination of the α and β carbons from **7a** was found to be the lowest energy pathway. As the S and C$^\gamma$ of **7a** approach each other the bicyclic isomer **8a** is formed. After cleavage of the C–S bond of the four-membered ring to form **9a**, the C_2H_2 moiety undergoes, consecutively, a rotation and a *cis–trans* isomerization to form the ion–molecule complex, **10**, which eventually dissociates to the thiophene radical cation (TP$^{+\bullet}$) and C_2H_2. This pathway appears to be the lowest energy pathway for the loss of C_2H_2, whose energy profile is shown in Fig. 1. The alternative pathway via **9d**, where the *cis–trans* isomerization occurs before the rotation of the C_2H_2 moiety, is energetically less favored.

We found other pathways for the loss of C_2H_2 from **7b**, which resulted in the elimination of the αβ, βγ, or γγ carbons (see Scheme 3). The isomerization pathways to **10** are similar to the lowest energy pathway via **7a**. As another pathway for the loss of C_2H_2, the 7-thia-norbornadiene radical cation (**14**) is formed from **2b** and isomerizes to **9a** (see Scheme 3). However, all these pathways are energetically much less favored than the lowest energy pathway.

3.2. Dissociation kinetics

Faulk et al. studied the dissociation kinetics of **1** using the time-resolved PI mass spectrometry (TPIMS), time-resolved photodissociation (TRPD)-ICR, and tandem mass spectrometry (MS/MS) [11]. Their results are summarized as follows. The RRKM model calculation was carried out assuming one-step dissociation for each of the losses of CS and C_2H_2. They could fit their TRPD and TPI data with the RRKM modeling using a very loose TS ($\Delta S^{\ddagger}_{1000\,K}$ = 14 eu (= 59 J mol^{-1} K^{-1})) and a critical energy of 3.2 eV for the loss of CS, and a tighter TS ($\Delta S^{\ddagger}_{1000\,K}$ = 2.74 eu) and a critical energy of 2.9 eV for the loss of C_2H_2. The two RRKM rate-energy curves crossed at $k \approx 4 \times 10^5$ s^{-1} and $E_{\mathbf{1a}} \approx 4.4$ eV. The loss of C_2H_2 was favored below 4.4 eV and the loss of CS above. They observed three metastable transitions in the MS/MS experiment: losses of H•, C_2H_2, and CS. On the other hand, the loss of SH• is one of the major dissociation channels in the EI spectrum. The relative abundances of the M$^{+\bullet}$, [M−H]$^+$, [M−SH]$^+$, [M−C_2H_2]$^{+\bullet}$, and [M−CS]$^{+\bullet}$ peaks in the reported 70-eV EI mass spectrum of thiophenol are 100, 24, 12, 14, and 31, respectively [8]. This suggests that the critical energy

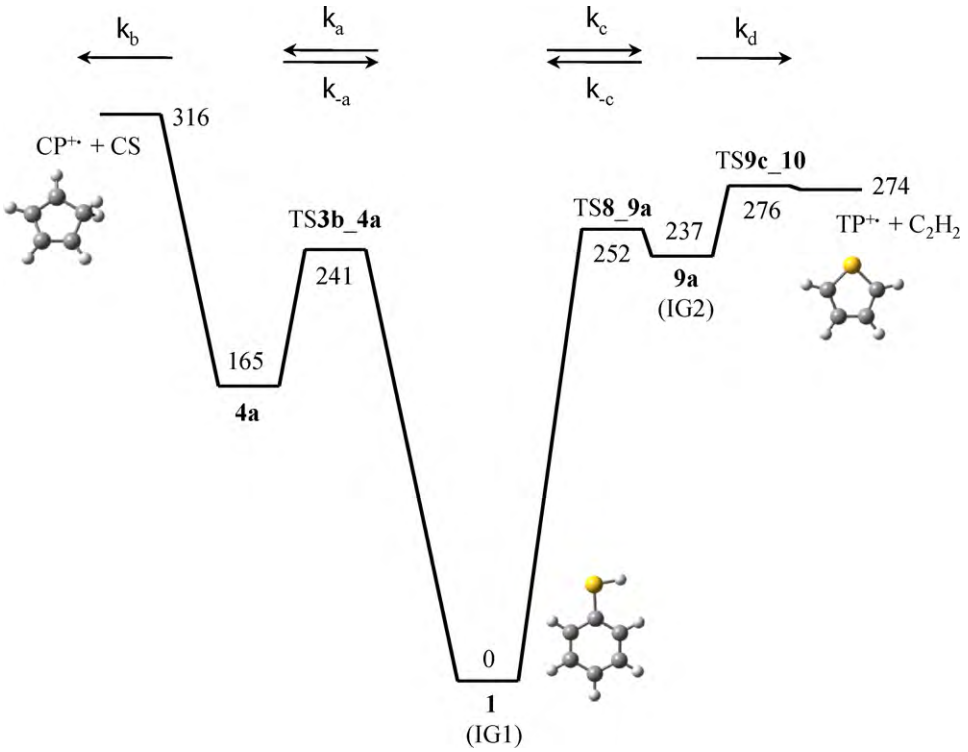

Fig. 2. Simplified potential energy diagram for the losses of CS and C_2H_2 from **1**, which was used for RRKM model calculations. IG1 includes **1**, **2a**, **2b**, **3a**, **3b**, **7a**, and **8** and IG2 includes **9a**, **9b**, and **9c**. See text for details. The energies are presented in kJ mol^{-1}.

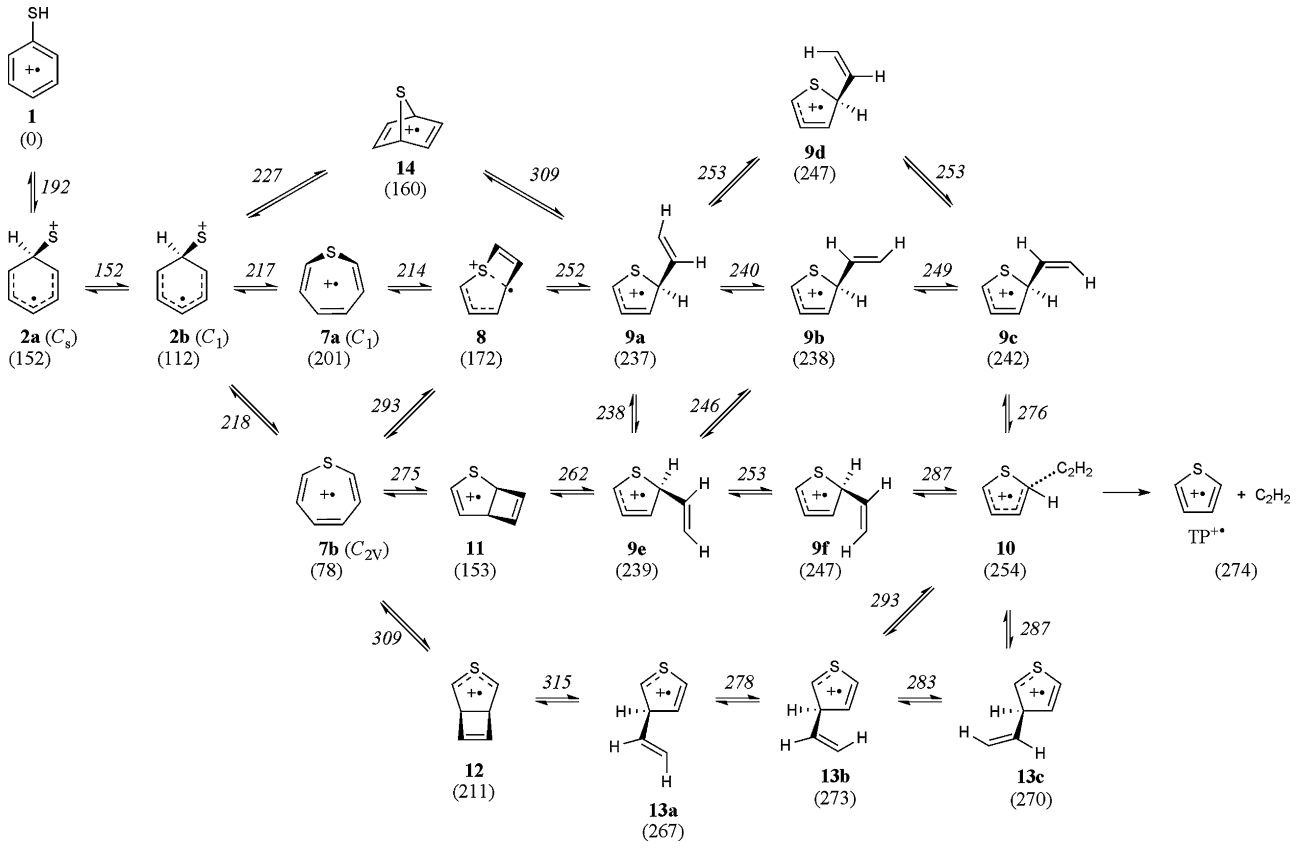

Scheme 3. The pathways for the loss of C_2H_2 from **1** obtained from G3//B3LYP calculations. The calculated relative energies presented in kJ mol^{-1} are shown in the parentheses for the stable species and next to the arrows for the TS's.

for the loss of SH• is higher than the other three channels observed in the metastable ion decomposition because a 70-eV EI spectrum includes dissociations of the molecular ions having internal energies higher than the metastable ions. These experimental results indicate that the loss of C_2H_2 is the only dissociation channel near the reaction threshold, and as the energy increases the other channels are opened in the following order: losses of CS, H•, and SH•. The order of appearance of the dissociation products determined experimentally agrees with the order of their thermodynamic stabilities calculated here (Table 1).

A kinetic analysis was carried out with RRKM model calculations to examine the competitive losses of C_2H_2 and CS on the basis of the obtained PES. Since dozens of intermediates are involved in the losses of C_2H_2 and CS, it is better for gaining an insight into the kinetics to use an approximate reaction scheme rather than to consider the complicated pathways thoroughly. We considered the lowest energy pathway only to simplify the PES. Since the isomerization barriers from **1** to **3b** and to **8** lay lower than either TS**3b_4a** or TS**8_9a** (see Fig. 1), it was assumed that the interconversion among **1** and six intermediates, **2a**, **3a**, **3b**, **2b**, **7a**, and **8** occurred rapidly before the next isomerization to either **4a** or **9a**, and hence this seven-well potential was approximated as a one-well potential. This was confirmed by calculating the RRKM rate constants for the individual isomerization steps. We will denote these interconvertible intermediates including **1** as Ion Group 1 (IG1). Because the ion–molecule complex **6a** was very unstable, its presence could be ignored kinetically in the pathway from **4a** to CP$^{+\bullet}$ + CS. Similarly, the three-well potential consisting of intermediates **9a**, **9b**, and **9c** (denoted as IG2) was treated as another one-well potential. The final intermediate to eliminate C_2H_2, **10**, was ignored because the dissociation step occurred very rapidly compared to the reverse isomerization to **9c**. Then, the two competitive dissociation channels occurring along with the lowest energy pathway are simplified as following equations and the PES shown in Fig. 2.

$$\mathrm{IG1} \underset{k_{-a}}{\overset{k_a}{\rightleftharpoons}} 4a \xrightarrow{k_b} \mathrm{CP}^{+\bullet} + \mathrm{CS} \tag{3}$$

$$\mathrm{IG1} \underset{k_{-c}}{\overset{k_c}{\rightleftharpoons}} \mathrm{IG2} \xrightarrow{k_d} \mathrm{TP}^{+\bullet} + \mathrm{C_2H_2} \tag{4}$$

In order to obtain the rate constants of reactions (3) and (4) ($k_{-\mathrm{CS}}$ and $k_{-\mathrm{C_2H_2}}$), those of the individual steps were calculated using the RRKM formalism in Eq. (1). The critical energies obtained from the G3//B3LYP calculations were used for the RRKM calculations (see Fig. 2). Because the six intermediates in IG1 were much less stable than **1**, their contributions to the density of the reactant states (the denominator in Eq. (1)) were ignorable, and hence only the parameters of **1** were used in the calculations of k_a and k_c together with the parameters of TS**3b_4a** and TS**8_9a**, respectively. On the other hand, all the contributions of the three intermediates in IG2 were included in the calculations of k_{-c} and k_d because their stabilities were similar. TS**8_9a** and TS**9c_10** were taken as the TSs in their respective calculations. The path degeneracy (σ in Eq. (1)) of 2 was used in the calculation of k_a because of the doubly degenerate pathway from **3b** to **4a**. Also $\sigma = 2$ was used for k_b because the two pathways for loss of CS from **4a** via either **6a** or **6b** were almost energetically identical (see Scheme 2). $\sigma = 1$ was used for the other rate constants. One uncertainty in the calculation of k_b was the set of parameters of the TS for the dissociation step in reaction (3), **4a** → CP$^{+\bullet}$ + CS, which occurred without a reverse barrier. The RRKM rate constants generally do not depend on the individual vibrational frequencies but on the $\Delta S^{\ddagger}$. Therefore, the frequencies for this TS were adjusted so that the calculated $k_{-\mathrm{CS}}$ curve, described below,

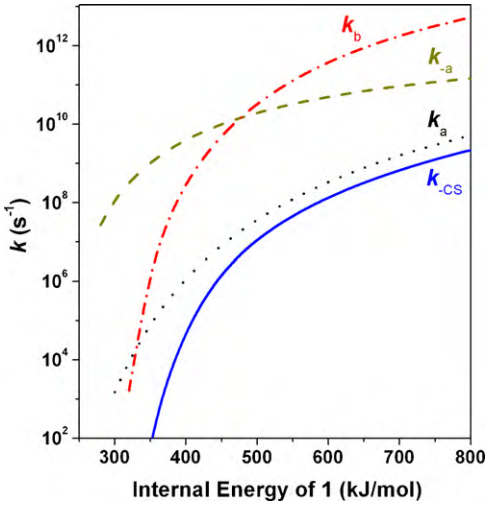

Fig. 3. Theoretical rate-energy dependence for the individual reaction steps in reaction (3) and for k_{-CS}. The rate constants for the individual reaction steps were calculated using the RRKM formalism.

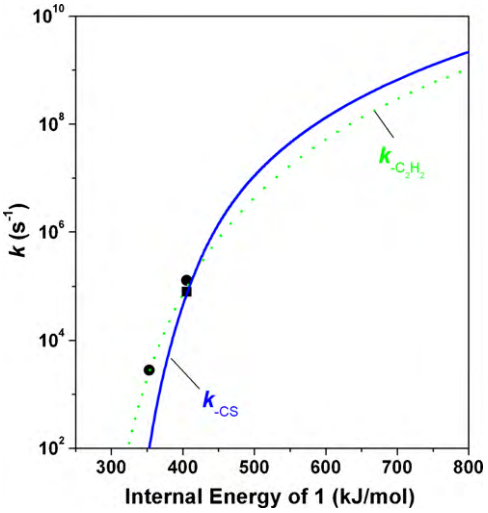

Fig. 5. Rate-energy dependence for k_{-CS} and $k_{-C_2H_2}$. Solid and dot curves are the result of RRKM model calculations for k_{-CS} and $k_{-C_2H_2}$, respectively. Rectangular and circular points are the TRPD-ICR result [11] for k_{-CS} and $k_{-C_2H_2}$, respectively.

fit the TRPD experimental data. The $\Delta S^{\ddagger}_{1000\,K}$ calculated from the frequencies was 7.7 eu, which was a reasonable value for a loose TS (see Table S3 in the supplementary material for the frequencies used in the RRKM calculations). The $\Delta S^{\ddagger}_{1000\,K}$ values for the other steps were calculated for comparison purposes. They were −2.5, −5.7, −1.4, −4.6, and 3.8 eu for the steps corresponding to k_a, k_{-a}, k_c, k_{-c}, and k_d, respectively. This indicates that the final dissociation steps in the two competitive reactions occur via loose TSs, while the other isomerization steps via tighter TSs. The RRKM rate-energy curves calculated for the individual steps are shown in Figs. 3 and 4.

The rate equations for reactions (3) and (4) could not be analytically solved. The coupled differential equations were numerically solved using the MATLAB program in order to obtain k_{-CS} and $k_{-C_2H_2}$, of which method is described in details elsewhere [6,20]. Their energy dependences thus obtained are shown in Figs. 3 and 4 and agree well with the TRPD experimental data as compared in Fig. 5. In Fig. 3, k_b increases more steeply than k_a or k_{-a} as the energy increases. This is because the former is determined by a loose TS while the latter two by tighter TSs as expected by their calculated $\Delta S^{\ddagger}_{1000\,K}$'s. k_{-CS} also increases more steeply than k_a in the low energy region, but behaves similarly to k_a in the high energy region. This means that the dissociation step characterizes the k_{-CS} curve pattern at low energies up to the crossing point between the k_b and k_{-a} curves, while the isomerization step does at high energies. On the other hand, the increasing pattern of $k_{-C_2H_2}$ is similar to k_c and their differences at the same energies are small as shown in Fig. 4. This means that the reverse isomerization and dissociation step, occurring very rapidly, can be almost neglected kinetically.

Both the losses of H• and SH• are energetically less favored than the loss of CS or C_2H_2. However, the former two become important as the energy increases because the direct loss of H• or SH• from **1** occurs via a loose TS. It is expected that the direct loss of H• is more favored than the loss of SH• when assuming similar looseness for the corresponding TSs because the critical energy for the former is smaller than that for the latter. In addition, the loss of H• can occur from isomers other than **1**, such as **2a**, **2b**, and **3a**, which contributes to its high abundance observed in the EI spectrum.

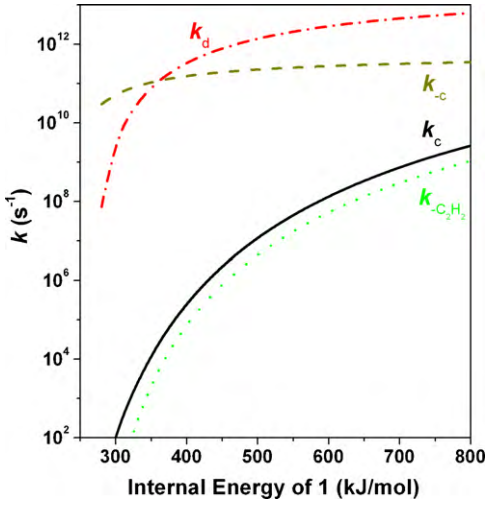

Fig. 4. Theoretical rate-energy dependence for the individual reaction steps in reaction (4) and for k_{-CS}. The rate constants for the individual reaction steps were calculated using the RRKM formalism.

3.3. Comparison with the phenol and phenylphosphine molecular ions

The gas phase chemistry of thiophenol has often been compared to phenol. For instance, their photodissociation dynamics [21] and metal ion mediated dissociations [22] were investigated. The loss of CO is the only primary dissociation channel for the phenol molecular ion as mentioned above. The PES for the loss of CO to form CP^{+}• obtained by the B3LYP/6-311++G(d,p) calculations was reported by Le et al. [7]. We obtained the G3//B3LYP energies for selected species based on the PES for comparison purposes (Table 2). The 1,3-H shift is the rate-limiting step in the loss of CO and the corresponding TS lies much higher than CP^{+}• + CO. The other possible channels such as losses of H•, OH•, and C_2H_2 from the phenol ion are energetically less favored than the loss of CO. Their endoergicities calculated via the G3//B3LYP method are 366, 433, and 315 kJ mol^{-1}, respectively, when their counter ions are the phenoxylium, phenylium, and furan cation. These are higher than the barrier (288 kJ mol^{-1}) for the1,3-H shift that limits the rate of loss of CO. Similarly, the 1,3-H shift through two consecutive 1,2-H shifts in the loss of CS from **1** occurs much lower than the other products. However, the loss of CS competes with the other channels because the final dissociation step, which lies much higher than the rearrangement steps, is the rate-limiting step. Faulk et al. demonstrated

Table 2
The calculated energies and relative abundances (RAs) in the EI mass spectrum (EIMS) for selected reactions of some $C_6H_5XH_n^{+\bullet}$ ions.

$M^{+\bullet}$	G3//B3LYP energy relative to $M^{+\bullet}$, kJ mol^{-1} [a]						RA in EIMS, % [b]	
	$[M-H]^+$ [c] + $H^\bullet$	$CP^{+\bullet}$ + CXH_{n-1} [d]	TS for 1,2-H shift [e]	TS for *ipso*-to- *ortho*-H shift [e]	TS for 1,3-H shift [e]	Highest barrier in the lowest energy pathway to form $CP^{+\bullet}$	$[M-H]^+$	$CP^{+\bullet}$
$C_6H_5OH^{+\bullet}$	366	116 (CO)	308	270	288	288	0	39
$C_6H_5SH^{+\bullet}$	333	316 (CS)	192	177	222	278	23	28
$C_6H_5PH_2^{+\bullet}$	236	232 (HCP)	115	120	211	237	22	6

[a] Ref. [6] for $C_6H_5PH_2^{+\bullet}$. The values for the others were calculated in this work.
[b] Ref. [8].
[c] Six-membered ring ion, $C_6H_5XH_{n-1}^+$.
[d] The neutral product is denoted in the parentheses.
[e] See Scheme 1 for definition.

that the significant difference between the formation of $CP^{+\bullet}$ from the phenol ion and **1** was due to the special stability of CO [11].

In the primary dissociation of the phenylphosphine molecular ion, which is isoelectronic with **1**, the formation of $CP^{+\bullet}$ by loss of HCP is not among the major dissociation channels. The $[M-H_2]^{+\bullet}$ peak is the base peak in the EI spectrum. The calculated G3//B3LYP critical energy (168 kJ mol^{-1}) for the loss of H_2 is much lower than those for the losses of HCP and $H^\bullet$ (see Table 2). Even though the barriers for the consecutive 1,2-H shifts, the early steps in the pathway to form $CP^{+\bullet}$, lie much lower than the other critical steps in the other channels (similar to the case of the phenol ion or **1**), the rate is determined at a late step characterized by a tight TS lying higher than the others. This makes the formation of $CP^{+\bullet}$ less important in the dissociation of the phenylphosphine ion, which is differently from the other two $C_6H_5XH^{+\bullet}$ ions.

4. Conclusions

To our knowledge, the PES of **1** was obtained by quantum chemical calculations for the first time. Several rearrangement pathways were determined for the losses of CS and C_2H_2 from **1**. Various types of intermediates including the seven- and five-membered ring isomers, bicyclic isomers, and ion–molecule complexes were involved in the dissociation. Similar to the other $C_6H_5XH_n^{+\bullet}$ ions, the 1,2 shift of the α-H and subsequent 1,2-H shift played important roles in the ring expansion and contraction, resulting in the competitive losses of CS and C_2H_2. The kinetic analysis predicted a crossover between the rate-energy curves for the two competitive channels, which agreed with previous experimental results. The rate of the loss of CS was mainly characterized by the final dissociation step occurring through a loose TS at low energies, while a tighter TS to form the five-membered ring intermediate **4a** limited the rate at high energies. On the other hand, the rate of the loss of C_2H_2 was mainly characterized by a tight TS to cleave the C–S bond of the bicyclic intermediate **8** at the whole energy range of our interest. The subsequent fast isomerization and dissociation steps hardly affected the rate. The proposed rearrangement mechanisms will be useful in the future mechanistic studies on ring expansion, contraction or opening of other aromatic molecular systems.

Acknowledgments

This work was supported by a National Research Foundation of Korea Grant funded by the Korean Government (2009-0072347). The authors would like to thank Bo Ram Kim for her assistance in preliminary calculations.

Appendix A. Supplementary data

Supplementary data associated with this article can be found, in the online version, at doi:10.1016/j.ijms.2010.07.005.

References

[1] C. Lifshitz, Y. Gotkis, A. Ioffe, J. Laskin, S. Shaik, Int. J. Mass Spectrom. Ion Process. 125 (1993) 7.
[2] J.C. Choe, J. Phys. Chem. A 110 (2006) 7655.
[3] J.C. Choe, Int. J. Mass Spectrom. 237 (2004) 1.
[4] M.T. Nguyen, in: Z. Rappoport (Ed.), The Chemistry of Anilines, Wiley, New York, 2007.
[5] J.C. Choe, N.R. Cheong, S.M. Park, Int. J. Mass Spectrom. 279 (2009) 25.
[6] S.Y. Kim, J.C. Choe, Int. J. Mass Spectrom. 294 (2010) 40.
[7] H.T. Le, R. Flammang, P. Gerbaux, G. Bouchoux, M.T. Nguyen, J. Phys. Chem. A 105 (2001) 11582.
[8] NIST Chemistry WebBook, NIST Standard Reference Database Number 69, in: P.J. Linstrom, W.G. Mallard (Eds.), National Institute of Standards and Technology, Gaithersburg MD, 20899. http://webbook.nist.gov (retrieved 17.05. 2010).
[9] D.G. Earnshaw, G.L. Cook, G.U. Dinneen, J. Phys. Chem. 68 (1964) 296.
[10] L. Stambolija, D. Stefanović, Org. Mass Spectrom. 7 (1973) 1415.
[11] J.D. Faulk, R.C. Dunbar, C. Lifshitz, J. Am. Chem. Soc. 112 (1990) 7893.
[12] J.D. Faulk, R.C. Dunbar, J. Phys. Chem. 93 (1989) 7785.
[13] M.J. Frisch, G.W. Trucks, H.B. Schlegel, G.E. Scuseria, M.A. Robb, J.R. Cheeseman, G. Scalmani, V. Barone, B. Mennucci, G.A. Petersson, M.C.H. Nakatsuji, X. Li, H.P. Hratchian, A.F. Izmaylov, J. Bloino, G. Zheng, J.L. Sonnenberg, M. Hada, M. Ehara, K. Toyota, R. Fukuda, J. Hasegawa, M. Ishida, T. Nakajima, Y. Honda, O. Kitao, H. Nakai, T. Vreven, J.A. Montgomery Jr., J.E. Peralta, F. Ogliaro, M. Bearpark, J.J. Heyd, E. Brothers, K.N. Kudin, V.N. Staroverov, R. Kobayashi, J. Normand, K. Raghavachari, A. Rendell, J.C. Burant, S.S. Iyengar, J. Tomasi, M. Cossi, N. Rega, J.M. Millam, M. Klene, J.E. Knox, J.B. Cross, V. Bakken, C. Adamo, J. Jaramillo, R. Gomperts, R.E. Stratmann, O. Yazyev, A.J. Austin, R. Cammi, C. Pomelli, J.W. Ochterski, R.L. Martin, K. Morokuma, V.G. Zakrzewski, G.A. Voth, P. Salvador, J.J. Dannenberg, S. Dapprich, A.D. Daniels, Ö. Farkas, J.B. Foresman, J.V. Ortiz, J. Cioslowski, D.J. Fox, Gaussian 09, Revision A. 02, Gaussian Inc., Wallingford, CT, 2009.
[14] A.G. Baboul, L.A. Curtiss, P.C. Redfern, J. Chem. Phys. 110 (1999) 7650.
[15] L.A. Curtiss, K. Raghavachari, P.C. Redfern, V. Rassolov, J.A. Pople, J. Chem. Phys. 109 (1998) 7764.
[16] T. Baer, W.L. Hase, Unimolecular Reaction Dynamics: Theory and Experiments, Oxford University Press, New York, 1996.
[17] T. Beyer, D.R. Swinehart, ACM Commun. 16 (1973) 379.
[18] S. Olesik, T. Baer, J.C. Morrow, J.J. Ridal, J. Buschek, J.L. Holmes, Org. Mass Spectrom. 24 (1989) 1008.
[19] S.G. Lias, J.E. Bartmess, J.F. Liebman, J.L. Holmes, L.R.D. Levein, W.G. Mallard, J. Phys. Chem. Ref. Data 17 (Suppl. 1) (1988).
[20] J. Seo, H.-I. Seo, S.-J. Kim, S.K. Shin, J. Phys. Chem. A 112 (2008) 6877.
[21] M.N.R. Ashfold, A.L. Devine, R.N. Dixon, G.A. King, M.G.D. Nix, T.A.A. Oliver, Proc. Natl. Acad. Sci. 105 (2008) 12701.
[22] M. Brönstrup, D. Schröder, H. Schwarz, Chem. Eur. J. 6 (2000) 91.